Microporous and Mesoporous Materials 384 (2025) 113453

Contents lists available at ScienceDirect

Microporous and Mesoporous Materials

journal homepage: www.elsevier.com/locate/micromeso

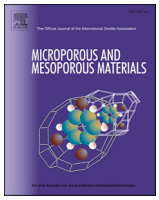

Green synthesis of functionalized sodalite ZIFs through mechanochemistry and their performance in CO_2 capture

Aljaž Škrjanc [a,b], Amalija Golobič [c], Matjaž Mazaj [a], Matej Huš [a,b,d,e], Blaž Likozar [a], Nataša Zabukovec Logar [a,b,*]

[a] National Institute of Chemistry, Hajdrihova 19, SI-1001, Ljubljana, Slovenia
[b] University of Nova Gorica, Vipavska 13, SI-5000, Nova Gorica, Slovenia
[c] Faculty of Chemistry and Chemical Technology, University of Ljubljana, Večna pot 113, SI-1000, Ljubljana, Slovenia
[d] Association for Technical Culture of Slovenia (ZOTKS), Zaloška 65, SI-1001, Ljubljana, Slovenia
[e] Institute for the Protection of Cultural Heritage of Slovenia (ZVKDS), Poljanska 40, SI-1001, Ljubljana, Slovenia

ARTICLE INFO

Keywords:
Mechanochemistry
Zeolitic imidazolate frameworks
Water adsorption
CO_2 adsorption
Liquid assisted grinding

ABSTRACT

Mechanochemical synthesis of Zeolitic imidazolate frameworks (ZIFs) has emerged as a compelling and environmetally conscious alternative to conventional solvothermal methods, especially when they rely on the use of toxic formamide-based solvents and excess of metal precursors or linkers. In this study, a facile liquid assisted grinding synthesis achieving high product yields with short synthesis times, have been introduced for a series of ZIFs with SOD topology featuring both single and mixed ligands with diverse functional groups. The phase pure and crystalline products with even particle size distribution and retained sorption performance confirmed the efficiency of mechanochemical synthesis as sustainable and viable approach for the optimisation and the design of a new ZIF archetypes. Deeper insights into the structural and CO_2 sorption capabilities was gained by a comparative quantum chemical calculations between a benchmark ZIF-8 and a newly synthesized isostructural analogue NICS-23, featuring an ester-functionalized imidazole ligand. The analysis revealed distinctive sorption characteristics of NICS-23, showcasing also its potential for gas separation processes with wet CO_2 involved. Findings highlight the advatages of mechanochemical synthesis in ZIF production as a facile green synthesis method over the longer solvothermal procedure, potentially allowing also for faster screening of functional materials.

1. Introduction

With a rising interest in different applications of Zeolitic imidazolate frameworks (ZIFs), a subgroup of Metal organic frameworks (MOFs), the environmental impact of synthesis of these materials has to be reduced as much as possible [1,2]. Most synthesis procedures for new materials still heavily rely on formamide-based solvents [2–9] such as dimethylformamide (DMF) and diethylformamide (DEF), coupled with large excesses of either metal precursors (MPs) [10] or linkers (L) [10,11]. To that end, different remediation strategies have thus far been implemented. The fastest is exchange of solvent for environmentally less problematic bio-based organic solvents[12–14], simple alcohols [10,15] or even water [16,17] wherever possible. Another is recycling of mother liquors after synthesis [11,18]. The ideal synthesis would have the least amount of solvent possible, or none at all, and would be done with stoichiometric ratios of metal to linker, with short synthesis times leading to phase pure products with high yields.

Mechanochemical synthesis of MOFs has lately become an example of such a synthesis by achieving high yields and short synthesis times, with the major drawback being the dependence on powerful enough mills. Optimised mechanochemical synthesis conditions allow for the use of oxide precursors [19,20], which lead to a significant reduction in cost as compared to metal salt precursors preferentially used in solvothermal synthesis.

Recent advances in mills have reduced the price of powerful enough devices for material synthesis down to where mechanochemical synthesis could be a very plausible alternative to classic solvothermal and precipitation-based laboratory scale synthesis approaches. Ball-milling (BM) in either vertical or horizontal mills has been the most utilised and has shown the most versatility for laboratory scale experiments,

* Corresponding author. National Institute of Chemistry, Hajdrihova 19, SI-1001, Ljubljana, Slovenia.
E-mail address: natasa.zabukovec@ki.si (N.Z. Logar).

https://doi.org/10.1016/j.micromeso.2024.113453
Received 3 October 2024; Received in revised form 2 December 2024; Accepted 4 December 2024
Available online 11 December 2024

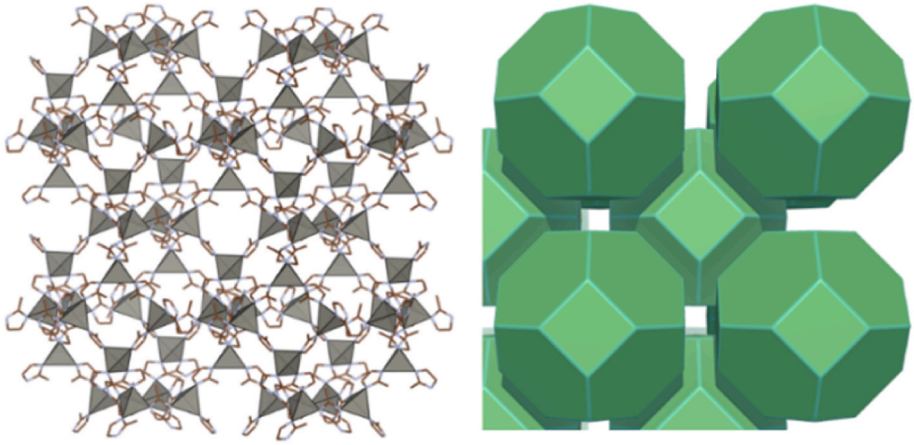

Fig. 1. Left: Zn tetrahedra connected with 2-methylimidazolate linkers into the SOD framework ZIF-8, Right: SOD tiling drawn with ToposPro and Gavrog.

Table 1
List of known single linker Zn SOD ZIFs.

Material	Alternative name	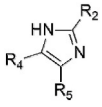			BET [m^2/g]	CO_2 uptake [mmol/g] at 1 bar and 25 °C	Ref.
		R2	R4	R5			
ZIF-7	MAF-3	Benzimidazole			/	1.5	[40]
ZIF-8	MAF-4	CH_3	H	H	1264–1630	0.97	[41]
ZIF-90		HCO	H	H	717	1.45	[4]
ZIF-94	SIM-1	H	HCO	CH_3	545	2.3	[26]
ZIF-65	NOF-1	NO_2	H	H	473–513	/	[42]
/	/	H	Cl	Cl	597	/	[28,43]
/	COK-17	H	Cl	Cl	500	2.5	[44]
/	/	X(Br, Cl, I)	H	H	/	/	[45]
/	NOF-2	H	NO_2	CH_3	/	/	[46]

with vertical mills in particular shown to be compatible with different spectroscopic techniques for in-situ measurements allowing for in depth mechanistic studies [19–25].

Due to the framework similarity to zeolites, for ZIFs, topology nomenclature from the zeolite field is used, with the most common ZIFs exhibiting the SOD[12,26–28] and RHO [5,29,30] topologies. Among these, the most studied and widely used ZIF is zinc 2-methylimidazolate with SOD topology named ZIF-8 (Fig. 1). To date, it has also been the most studied ZIF for mechanochemical preparation, with different research groups reporting various approaches using different precursors, mills and milling conditions [31].

The ball-mill synthesis of ZIFs can be grouped into two large categories: neat grinding (NG) and liquid assisted grinding (LAG), with possible further divisions regarding which metal precursors and proton transfer co-catalysts are used. Most commonly, the acetate ion is used as a proton transfer co-catalyst with synthesis using both acetate salts [32] and/or acetic acid solutions [23] as reported in the literature.

One of the potential adsorption applications that ZIFs have been widely tested for is carbon capture and storage, with most tests still largely focused on pure single-component CO_2 gas sorption. In addition to ZIF-8, several other ZIFs exhibit SOD framework topology (Table 1) and are among the most commonly tested for CO_2 adsorption due to their stable frameworks, with ZIF-90 and ZIF-94 exhibiting the most promising CO_2 capture performances among all as-prepared ZIFs, reportedly due to the presence of polar functional adehyde groups on the linkers. Additional improvements in CO_2 capture performance were recently achieved through additional mostly post-synthetic functionalization[4,33–36] approaches, which again were most commonly done on ZIFs with SOD topology, most notably ZIF-8 and ZIF-90. The functionalization included incorporation/nanoconfinement of ionic liquids, organic dyes, metal oxides, like MgO and ZnO or lithium cations as electron rich centres for trapping the CO_2 molecules. Another route to introduce polar functional groups ist the mixed linker (ML) approach, when the linker of interest does not form porous structures with the desired porosity/topology [37], here a linker is chosen that forms the desired framework and some of the second linker with the desired functionality is incorporated into the structure. If the direct synthesis route is not possible then a post synthethic linker exchange with the linker with desired functionality can also be performed [38,39].

Herein we report a facile LAG synthesis of a series of nine single- or mixed-linker SOD ZIFs (Fig. 2), with varying functional groups, of which four have not yet been reported. One of them, NICS-23, is the first as-synthesized ZIF with ester functional group on the ligand. In addition to structural characterization, potential drawbacks of LAG synthesis on structural properties, if compared to available solvothermal analogues, were evaluated, where the data was available. Finally, the prepared materials were assessed for their performance as sorbents for dry and wet CO_2, underscoring the significance of tailored functionalization for enhanced CO_2 capture applications, also possible by the use of mechanochemistry.

2. Experimental

2.1. Materials

2-Methyl imidazole (2MIM, 99 %), benzimidazole (BIM, 98 %), 2-imidazole carbaldehyde (HICA-L3, 97 %), Zinc acetate ($Zn(AcO)_2 \times {}_2H_2O$, 99 %), zinc oxide (ZnO, 99 %), N,N-dimethylformamide(DMF),

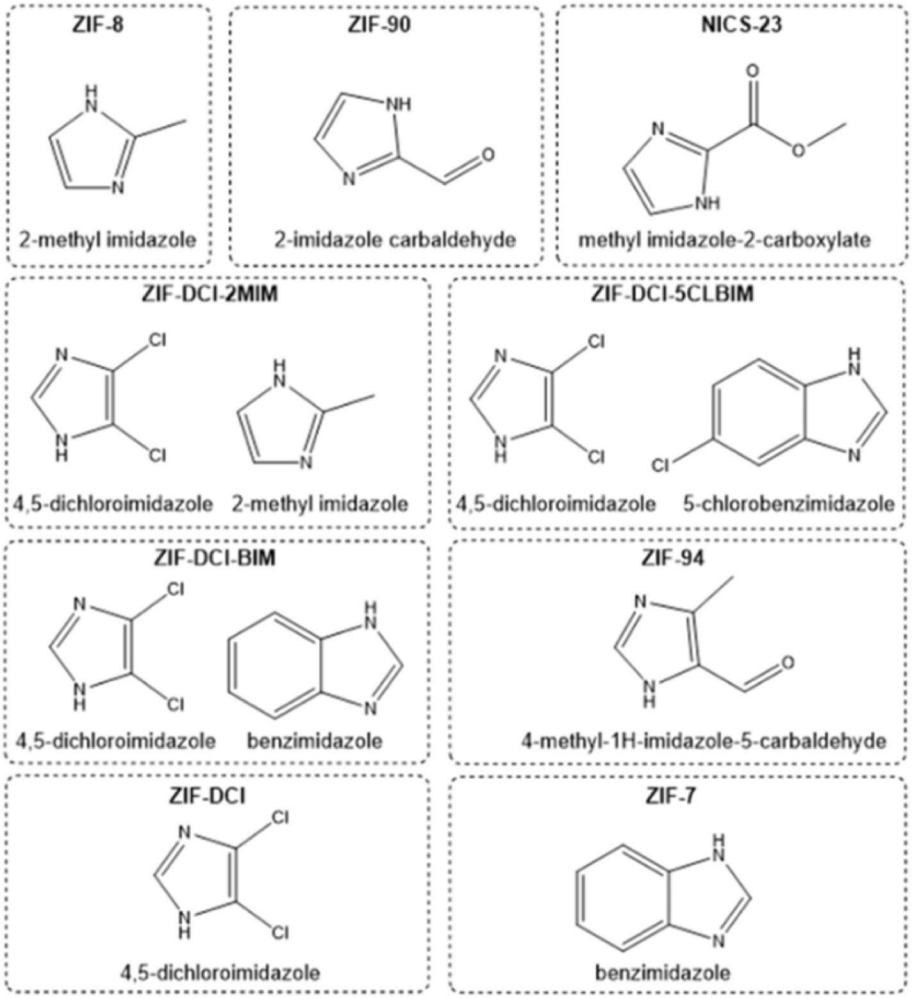

Fig. 2. ZIFs reported in this work, and their corresponding linkers.

Table 2
Synthesis conditions for BM ZIFs.

Sample	ZnO [mg]	Zn(AcO)2 × 2H2O [mg]	Linker [mg]	LAG solvent [μl]	Grinding jar volume [mL]	Grinding ball diameter [mm]	Time [min]	Frequency [Hz]	Known structure
ZIF-8	73.6	22.1	2-methyl imidazole; 164	GVL 100	10	10	30	30	YES
ZIF-90	73.6	22.1	2-imidazole carbaldehyde; 198	GVL 100	10	10	30	30	YES
NICS-23	146	44.2	methyl imidazole-2-carboxylate; 503	GVL 200	25	15	30	20	**NO**
ZIF-DCl-2MIM	73.4	22.2	4,5-dichloroimidazole; 137 2-methyl imidazole; 81	GVL 50 H_2O 50	10	10	30	30	**NO**
ZIF-DCl-5CLBIM	73.4	22.2	4,5-dichloroimidazole; 137 5-chlorobenzimidazole; 152.6	GVL 50 H_2O 50	10	10	30	30	**NO**
ZIF-DCL-BIM	73.3	21.9	4,5-dichloroimidazole; 136.5 Benzimidazole; 118	GVL 50 H_2O 50	10	10	30	30	**NO**
ZIF-94	73.2	21.9	4-methyl-1H-imidazole-5-carbaldehyde; 220	H_2O 100	25	15	45	20	YES
ZIF-DCL	72.8	21.9	4,5-dichloroimidazole; 274.2	DMF 50	10	10	45	30	YES
ZIF-7	81	/	Benzimidazole; 236	GVL 200 1M AcOH (aq) 200	10	10	15	30	YES

DCl(35 % in D_2O) and gamma-valerolactone (GVL) were purchased from Sigma Aldrich. Methyl imidazole-2-carboxylate (MICA, 97 %), 5-chlorobenzimidazole (5CLBIM, 97 %), 2-imidazole carbaldehyde (HICA-L1 and HICA-L2), 97 %) and 4-methyl-1H-imidazole-5-carbaldehyde (4MHICA, 97 %) were purchased form Fluorochem. 4,5-dichloroimidazole (DCIM, 98 %) was purchased from ABCR. Ethanol (EtOH, 96 %) was purchased from Stella TECH. DMSO-d6 was purchased from Eurisotop. Water was deionised in-house.

2.2. Mechanochemical synthesis

Table 2 shows the optimised reagent amounts and grinding conditions for the syntheses of selected ZIFs. In general, for the BM procedure, the metal precursors were added into a stainless-steel grinding jar,

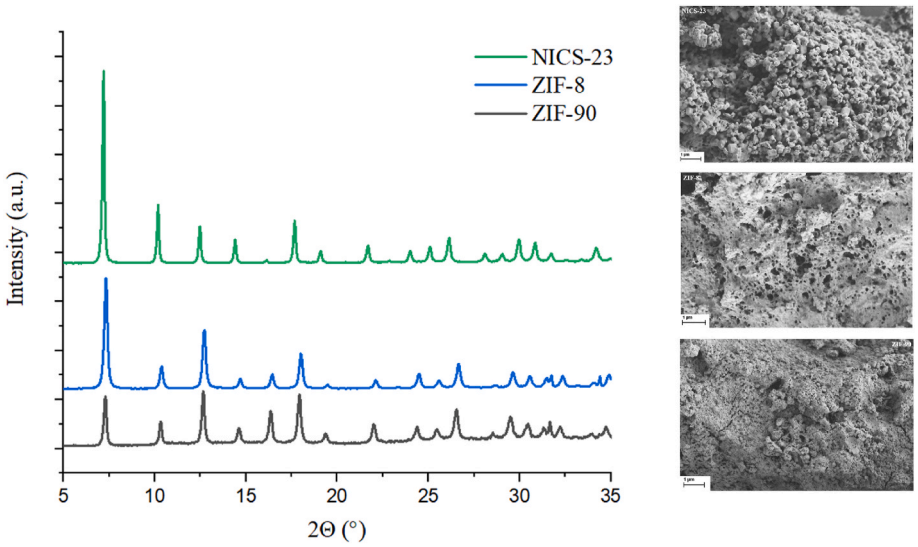

Fig. 3. PXRD of as prepared ZIF-90, NICS-23 and ZIF-8, SEM of ZIF-90 (bottom) ZIF-8 (middle) and NICS-23 (top). High resolution SEMs are available in SI (Figures S9.1-S9.3).

followed by linkers and the stainless-steel grinding balls and finally small amounts of LAG solvents were added; the jars were closed and milled using a Retsch MM400 vibrational mill. The products were obtained with yields in the range of 85–93 %, depending on the synthesis attempt. At the small scale used, the sample loss during removal from the grinding jar was difficult to keep consistent. The yields are in line with previously reported yields for mechanochemistry [47].

The as-synthesized samples were then placed in 25 mL glass vials, which were then topped up with MeOH. The vials were closed, shaken thoroughly and left to sit overnight. Afterwards, the solvent above the precipitated samples was removed using a pipette and the samples were dried in a 60 °C ventilator oven for an hour. The dried samples were then heated in a vacuum oven in a static vacuum at 150 °C overnight.

2.3. Instrumentation

Powder X-ray diffraction data (PXRD) qualitative analyses were recorded on a PANanalytical X'Pert PRO high-resolution diffractometer using $CuK_{\alpha 1}$ radiation (1.5406 Å) in the 2θ range from 5 to 50° (100 s per step 0.033° 2θ) with a fully opened X'Celerator detector. X'Pert High Score Plus was used for analysis of the collected PXRD, and for the unit cell parameter determination using Treor.

Nitrogen physisorption isotherms were recorded at −196 °C using the Anton Paar Quantachrome iQ3. Before the adsorption analysis, the samples were outgassed under vacuum for 10 h at 150 °C. The Brunauer–Emmett–Teller (BET) specific surface area was calculated from adsorption data in the relative pressure range from 0.005 to 0.02. The total pore volume (V_{total}) was calculated from the amount of N_2 adsorbed at P/Po = 0.97 and micropore volume from the t-plot ($p/p_0 = 0.15 - 0.3$).

Thermogravimetric analysis (TGA) was performed on a TA Instruments Q5000. The measurements were carried out in a continuous airflow (25 mL/min air), by heating samples from 25 °C to 650 °C at a rate of 10 °C/min.

Scanning electron microscope (SEM) images were taken using a Zeiss Supra 35 VP microscope with an electron high tension voltage of 1. kV and Aperture Size 30.00 μm.

CO_2, H_2O and humid CO_2 isotherms at 30 °C were collected on a Surface Measurement Systems DVS Vacuum. CO_2 and humid CO_2 isotherms were measured in the pressure range of 0–1 bar, with water vapour being added at the first step of the measurement. Afterwards, when the desired end relative humidity was reached, measurement was continued the same way as for dry CO_2.

Digestion liquid ^{1}H NMR was recorded using an AVANCE NEO Bruker 600 MHz spectrometer at room temperature. Approximately 1.5 mg of sample was digested in a mixture of DCl (35 %)/D_2O (0.1 ml) and diluted with DMSO-d6 (0.5 ml). Data analysis was performed using MestreNova software.

2.4. Computational details

To describe a new framework NICS-23 and a benchmark structure (ZIF-8), quantum chemical computations were performed using VASP 6.3.1 [48–50]. ZIFs were modelled with a plane wave basis set approach, using the RPBE exchange-correlation functional [51] in the projector-augmented-wave formalisms (PAW) [52]. To account correctly for dispersion interactions, which play a crucial role in the adsorption of apolar molecules, the D3 corrections by Grimme were used [53]. The calculations were performed with a gamma point sampling of the Brillouin zone, which was sufficient due to a large unit cell. A plane wave cutoff of 450 eV was used.

Both ZIFs were first fully optimised, allowing the unit cell parameters to change and the atom positions to adjust. Initial structural guesses were provided by the experimentally determined CIF structures and subjected to computational optimisation. Upon initial optimisation, a clean run was performed to ensure that the energies are computed consistently using plane waves commensurate with the actual unit cell. For the calculations of CO_2 adsorption, all possible sites were probed with one CO_2 molecule. Subsequently, the number of CO_2 molecules was increased until the average interaction became repulsive. Lattice parameters were not allowed to change during the adsorption calculations. For gaseous CO_2, the energy was computed in a cubic box of 20 x 21 × 22 Å to break the symmetry.

There are several approaches to modelling isotherms [54], depending on the system used. For instance, monolayer, two-layer and multilayer models have been fitted to empirical data [55] or grand canonical Monte Carlo simulations have been used [54,56], usually with force fields [57].

In our case, a simpler approach was used, as we are interested in trends between two different frameworks. On account of our system exhibiting a constant adsorption interaction, regardless of CO_2 coverage, we opt for a Langmuir isotherm, which relies on the ab initio free energy of adsorption, ΔG. The Gibbs free energy includes the interaction energy and includes the configurational entropy due to the distribution of

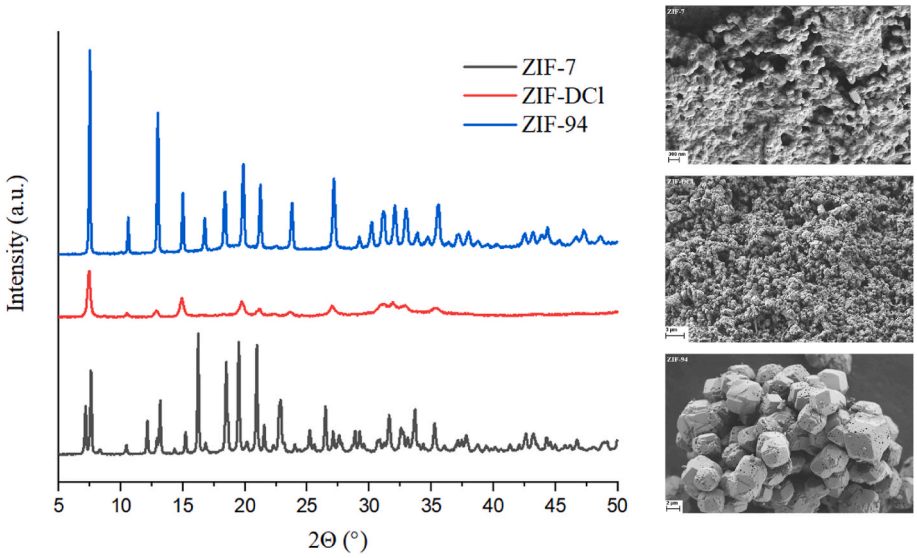

Fig. 4. PXRDs of as prepared ZIF-94, ZIF-7 and ZIF-DCl, SEM of ZIF-94 (bottom) ZIF-DCl (middle) and ZIF-7 (top). High resolution SEM are available in SI (Figures S9.4-S9.6).

adsorbed molecules and the vibrational contribution to the partition function of the adsorbate [54].

$$E_{ads} = E_{ZIF+CO_2} - E_{ZIF} - E_{CO_2}$$

And

$$\Delta G = \Delta E_{electronic} + \Delta E_{ZPE} - RT\ ln \frac{Q_{vib}^{adsorbed}}{Q_{Rot}^{gas} Q_{Trans}^{gas} Q_{Vib}^{gas}}$$

where the partition functions are defined as is customary [58].

3. Results and discussion

3.1. Synthesis and characterisation

3.1.1. LAG synthesis of ZIF-8, ZIF-90 and NICS-23

Initial synthesis attempts were derived from previously reported BM synthesis for ZIF-76 [47]. All initial synthesis attempts included a 10 % zinc acetate and 90 % zinc oxide metal precursor with either gamma-valerolactone (GVL) or water or a mixture of the two, making up the LAG solvent used (Tables 2 and SI Chapter S1). GVL, being a bio-based solvent, was previously shown to be a useful alternative to DMF in ZIF synthesis [12,47].

The reagent to grinding jar volume was kept at 1 mmol Zn per 10 mL grinding jar. The tested conditions led to the formation of PXRD phase pure NICS-23 (Fig. 3). In ZIF-8 PXRD pattern, two peaks observed at around 32° and 34° 2Θ can be ascribed to the (100) and (002) diffraction maxima of ZnO. At this point, it is worth mentioning that the SOD ZIFs form several different polymorphs (cubic, trigonal, monoclinic, etc.) originating from different synthesis and activation, external stimuli, etc. and leading to varying intensities in the PXRD patterns [59,60]. Representative patterns of activated cubic and trigonal polymorphs with assigned Miller indices of the peaks are in Supporting information Fig. S5.

While attempts at preparing ZIF-90 were successful, we encountered issues with repeatability between linkers from different batches and sources (Fig. S1). Additional optimisation attempts to increase the crystallinity of ZIF-90 with the problematic linker batch led to formation of a 2D layered imidazolate framework [61] (Fig. S1). On the other hand, the use of the HICA-L3 linker for ZIF-90 led to a highly crystalline ZIF-90 phase with some smaller impurities of another phase that we could not identify.

A newer batch of linker (HICA-L2) was purchased and with it ZIF-90 could be prepared. In all cases ZIF-90 BM synthesis seemed to be largely impacted by potential impurities in the commercially obtained linkers.

SEMs of the three ZIFs revealed the presence of small nanoparticles below 100 nm, which were agglomerated. SEM of ZIF-8 (Fig. 3) show that the crystallites are a few tens of nm in size and show large agglomeration. NICS-23 crystalized in irregularly sized octahedral crystallites (up to 100 nm in size) which again agglomerated (Fig. 3). ZIF-90 (Fig. 3) exhibits similar agglomerated small nanoparticles as observed for ZIF-8. The size of the primary particles is only slightly reduced, if compared to their solvothermal analogues [12,36].

The unit cell parameters were calculated (Table S1), and all phases are confirmed to be cubic with unit cell parameter *a* in the ranges reported for sodalite ZIFs.

NICS-23 was also successfully prepared solvothermally (SI Chapter S3) and its structure determined using PXRD data (CCDC deposition number 2300625). The reported ZIF is to our knowledge the first known ZIF with an ester group at the R2 position (Table 1), which opens up new chemistry of potential post-synthetic modification of ZIFs.

3.1.2. LAG synthesis of ZIF-DCl, ZIF-7 and ZIF-94

The remaining three single linker ZIFs, ZIF-DCl, ZIF-7 and ZIF-94 (Fig. 4), required further synthesis optimisation steps, as the frameworks linkers in combination with Zn tend to favour two stable phases, the RHO and SOD, and with 4,5-dichloroimidazole and zinc also additional stable phases that do not exhibit porosity.

Initial synthesis attempts of ZIF-94 led to the formation of the ZIF-93 with RHO topology or a mixture of the two phases. Variation in grinding jar size and frequency allowed for repeatable selective formation of ZIF-94 when using smaller amounts of reagents in a larger grinding vessel. Further optimisation steps included a variety of potential proton transfer co-catalysts, with addition of ammonia to the LAG solvent leading to selective formation of ZIF-94 when grinding larger amounts of reagents in the jars. As comparable crystallinity was achieved when milling a smaller amount of reaction mixture in larger jars, we decided to continue with the ammonia free synthesis route, to further increase atom economy and reduce environmental impact of the synthesis. SEM images (Fig. 4) of the prepared ZIF-94 show large cubic particles (5 μm) that seemed to have formed through fusion of smaller crystallites.

Attempts to prepare ZIF-DCl with GVL or water as LAG solvents led to formation of the RHO or a mixture of the RHO and lcs topologies, with NG leading to pure RHO with high crystallinity; following that, we

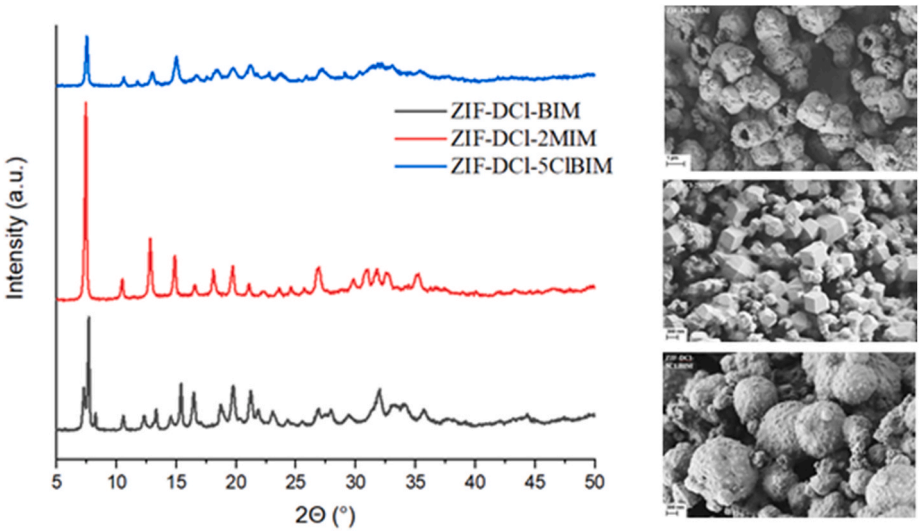

Fig. 5. PXRD of as prepared ML ZIF-DCl SOD samples, SEM of DCl-5ClBIM (bottom) ZIF-DCl-MIM (middle) and ZIF-DCl-BIM (top). High resolution SEM are available in SI (Figures S9.7-S9.9).

attempted the synthesis with DMF. LAG with DMF with short milling times led to the formation of a pure SOD phase with longer milling times leading to either RHO, lsc or a mixture of phases. Further attempts to increase crystallinity tended to result in formation of the lcs phase of ZIF-72. SEM images (Fig. 4) of the prepared ZIF-DCl show similar agglomerated nanoparticles of a few tens of nm in size as those of ZIF-8 and ZIF-90. Occasional plate-like impurities can be observed, which can be attributed to ZIF-72 impurities.

A similar alternate phase problem was observed with ZIF-7. Benzimidazole and zinc can form a well-known 2D layered structure [62], which we found to be the main product in a lot of our attempts. Using alternative zinc acid salts led to the formation of the RHO phase. ZIF-7 was then finally obtained (Fig. 4) after a large increase in LAG and using an acid solution together with GVL. This led to formation of well-defined octahedral crystallites of up to 200 nm in size, which were further agglomerated, as observed on SEM (Fig. 4). The prepared ZIF-7 resulting from the synthesis attempts showed low thermal and chemical stability leading to additional PXRD diffraction peaks, which due to low crystallinity we could not confidently assign to the close pore phase of ZIF-7 [63]. Due to its low thermal stability, we decided not to continue with sorption tests with ZIF-7(Fig. S2).

The calculated unit cell parameters of the as synthesized ZIF-94 and ZIF-DCl both exhibited cubic symmetry, while ZIF-7 crystalized in the trigonal symmetry. The unit cell parameters of all three were within the reported values (Table S1).

3.1.3. *LAG synthesis of mixed-linker SOD ZIFs*

Literature reported success in the solvothermal preparation of mixed linker (ML) COK-17/ZIF-7 [64], a conformational polymorph of the SOD ZIF-DCl; this led us to investigating the possible formation of ML SOD frameworks consisting of 4,5-dichloroimidazole(DCIM) and either 2-methylimidazole(2MIM), benzimidazole(BIM) or 5-chrolobenzimidazole(5CLBIM). The 2MIM and 5CLBIM mixed linker ZIFs exhibit a classic cubic SOD PXRD pattern (Fig. 5), with the BIM sample exhibiting the characteristic SOD-trigonal pattern of ZIF-7 and COK-17 with an additional peak that can be assigned to a layered benzimidazole phase [62] that we have found to appear in most BIM mechanochemical synthesis attempts.

We decided to continue with activation and nitrogen sorption to check if the second phase has any impact on sorption properties of the rest of the bulk material and found no significant decrease in S_{BET} to that reported for the parent COK-17 [44].

The samples exhibit varying morphologies: ZIF-DCl-2MIM crystallised in well-defined cubic particles (100–400 nm) which are agglomerated (Fig. 5), while ZIF-DCl-5ClBIM formed spherical agglomerates (1 μm) (Fig. 5). SEM images (Fig. 5) of ZIF-DCl-BIM show large cubic like particles made out of agglomerated (1–2 μm) smaller crystallites (~300 nm), similar to ZIF-94; what is also interesting is that the cubes appear to be hollow. Variation in ratio of the linkers led to a mixture of the RHO and SOD phases when increasing the amount of DCIM (Fig. S3).

The unit cell parameters were determined (Table S1), and again here for ZIF-5ClBIM and ZIF-2MIM the cubic symmetry was observed, while ZIF-DCl-BIM, same as ZIF-7, crystalized in the trigonal unit cell.

The activated ML samples were then analysed with acid digestion liquid ^{1}H NMR (Fig. S5) to determine the final ratios in the prepared frameworks. In all cases, the determined ratio between linkers was determined to be the initial 1:1. This was expected as the phase only forms when a 1:1 ratio is used in synthesis. The herein prepared new ML phases further highlight that mechanochemistry can sometimes not only be used to prepare known phases but can be the only route towards preparation of new phases. As synthesized single linker samples were also analysed with 1H NMR (Fig. S5) to check if any chemical changes occurred to the linkers during synthesis. The NMR show the peaks for water, DMSO, and for the linker, with some residual solvent peaks visible in the 0–2.5 ppm region. Together with no visible colour changes of the samples compared to the starting materials, we can assume that no decomposition occurred.

3.2. *Sorption properties*

The prepared samples were activated and the nitrogen isotherms collected (Supporting information S1.4.1) to confirm the samples permanent porosity, NLDFT pore size distribution and to determine their specific surface area. The activated samples were also analysed with TGA (Fig. S5) and no additional mass losses, attributed to remaining solvents or other less volatile compounds, were observed in all cases. Furthermore, the CO_2, H_2O and model 50 % RH CO_2 isotherms were collected (Fig. 6, Figure S8, S1.4.1). PXRD analysis of samples after sorption was performed as in all cases except for ZIF-90, no difference in PXRD was observed (Fig. S4). The loss in crystallinity after water sorption was expected for ZIF-90, as we have already observed this previously for solvothermally prepared ZIF-90 [65].

All samples S_{BET} values (Table 3) were within the range of literature reported values for their solvothermal analogues, if available (listed in Table 1), proving that LAG can be an effective and facile green synthesis

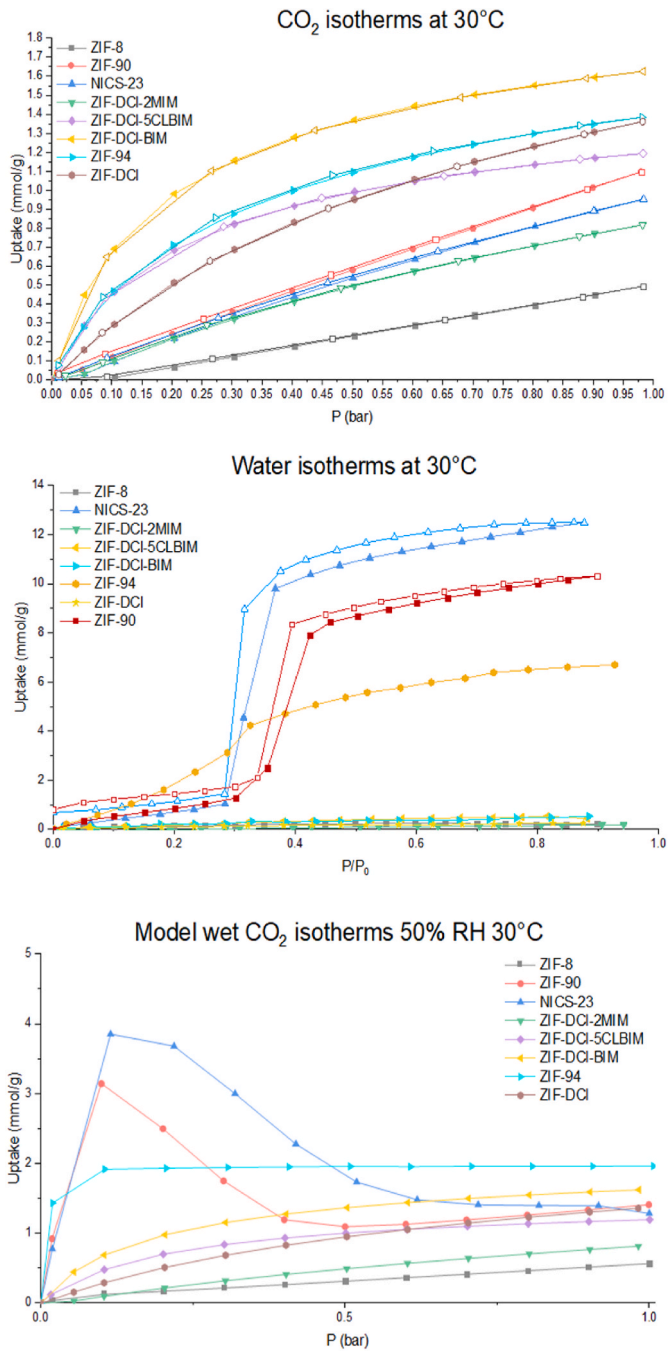

Fig. 6. CO_2, water and model wet CO_2 adsorption isotherms at 30 °C for the SOD ZIFs.

method over the longer solvothermal procedure, potentially allowing also for faster screening of functional materials. The obtained results follow the general trends of bulkier ligands leading to lower S_{BET} and V_{micro}.

The CO_2 uptake (Fig. 6, Table 3) further confirmed the sorption performance of mechanochemically prepared SOD ZIFs and also showed the expected trends of: more polar functional groups→ stronger interactions→ higher CO_2 uptake, where not limited by (non)porosity. While 5CLBIM would potentially lead to the highest interactions in the SOD framework, due to the presence of polar groups and aromatic rings that are also reported to possibly enclose CO_2 molecules, if properly stuck, the significant decrease in specific surface area limits the maximum adsorption. ZIF-94, ML ZIF-DCl and ZIF-DCl (Fig. 6) all exhibit a Langmuir type isotherm, which is indicative of stronger dipole interactions with CO_2 as compared to the linear isotherms of the other ZIFs.

While comparison with other ZIFs is slightly biased due to most reported CO_2 uptakes being measured at 25 °C, while ours are at 30 °C, we can conclude that mechanochemically prepared samples that have known solvothermally prepared counterparts perform very similarly, expect for samples where some loss of porosity is observed, there the uptake is comparatively slightly lower. NICS-23 BM and solvothermally prepared (ST) exhibit the same linear isotherms with very similar uptakes (Fig. S7), the same Langmuir type isotherm is also observed for BM and ST ZIF-94, except due to the lower porosity a lower uptake is observed for BM ZIF-94.

Based on presented results, we can estimate that the phase ZIF-DCl-BIM could potentially have the second or third highest uptake of ZIFs.

Water isotherms (Fig. 6) for ZIF-90, and NICS-23 showed the expected inflection points at around 30–35 % RH. ZIF-94 on the other hand exhibited more of a type II isotherm. All the hydrophilic frameworks showed a similar small hysteresis The rest of the frameworks were highly hydrophobic resulting in almost no water adsorption (less than 1 wt%).

In the model wet CO_2 system, the hydrophobic materials exhibit no or a small change in CO_2 uptake compared to dry CO_2 adsorption. The series of hydrophilic ZIFs (ZIF-90, NICS-23 and ZIF-94), demonstrated why studying of wet gas mixtures is important. ZIF-94 fully saturated with water leads to no additional adsorption at higher gas pressure, contrary to published results from breakthrough curved for the solvothermally prepared ZIF-94 [66]. The other two ZIFs isotherms begin with a large increase in mass thanks to water adsorption followed by gradual mass loss at higher CO_2 leading to isotherms with negative slopes. The negative slope could be indicative of preferential adsorption of CO_2 on the framework under these model conditions. All three hydrophilic materials exhibited low selectivity towards CO_2 in the lower pressure ranges, somewhat narrowing the field of use for these materials to higher CO_2 pressures for use with wet CO_2 or limiting the max humidity to 30 % requiring drying steps before adsorption.

Table 3
Results of sorption tests for BM SOD ZIFs.

Sample	S_{BET} [m^2/g]	V_{micro} [mL/g]	V_{total} [mL/g]	CO_2 uptake [mmol/g]	Wet CO_2 [mmol/g]	H_2O uptake [mmol/g] (wt%)
ZIF-8	1451	0.56	0.61	0.5	0.57	<0.5 mmol (0.4)
ZIF-90	626	0.24	0.41	1.09	/[c]	10.3 (18.6)
NICS-23	732	0.24	0.35	0.95	/[c]	12.5 (22.5)
ZIF-DCl-2MIM	669	0.21	0.313	0.82	0.83	<0.5 mmol (0.3)
ZIF-DCl-5CLBIM	90[a]	/[a]	/[a]	1.19	1.20	<0.5 mmol (0.8)
ZIF-DCl-BIM	422	0.14	0.20	1.63	1.57	<0.5 mmol (0.8)
ZIF-94	478	0.16	0.23	1.38	/[b]	6.7 (12.1)
ZIF-DCl	541	0.19	0.26	1.36	1.34	<0.5 mmol (0.45)

[a] BET determined from 11 sorption points collected, whole isotherm could not be measured.
[b] saturated with water.
[c] adsorption of both adsorbates.

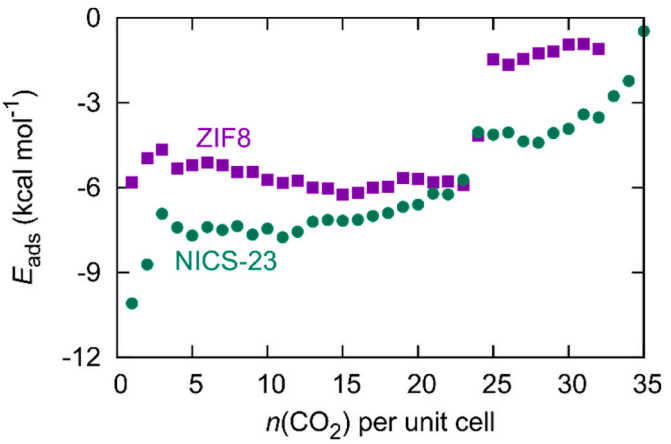

Fig. 7. Differential adsorption interaction per one CO_2 molecule as a function of loading.

3.3. Computational investigation into sorption in NICS-23 and ZIF-8

To ascertain that the computational approach is valid, a benchmark material ZIF-8 was studied along with the new frameworks of NICS-23. The optimised cubic cell parameters of ZIF-8 and NICS-23 are 16.86 Å and 17.20 Å, respectively, which is within 0.9 % of the experimentally determined values.

Among different sites probed for CO_2 adsorption, the strongest interaction is −5.8 kcal mol^{-1} with ZIF-8 and –10.1 kcal mol^{-1} with NICS-23. This roughly correlates with the experimentally determined sorption ability of both materials, which is stronger for NICS-23.

The CO_2 adsorption interaction with ZIF-8 has previously been computed with slightly different parameters and was found to match our predictions (−5.9 kcal mol^{-1} by Fischer and Bell [67] and −5.01 kcal mol^{-1} by Paudel et al. [68]). The corresponding Gibbs free energies of adsorption at 1 bar were calculated to be +4.62 and + 0.01 kcal mol^{-1}, respectively.

The most favourable adsorption site for CO_2 in ZIF-8 is parallel to the imidazole ring, approximately 3.3 Å away, which is consistent with the work by Fischer and Bell [67]. On the other hand, sites close to the metal centre exhibit a strong repulsion. Consistent with the findings from Paudel et al. [68], we also observe that the differential interaction per one added CO_2 molecule decreases up to $n = 3$ and then fluctuates between 5 and 6 kcal mol^{-1} up to 23 CO_2 molecules per unit cell (Fig. 7), which corresponds to an uptake 8.4 mmol/g. This can be viewed as a maximum possible uptake at a high CO_2 pressure.

In NICS-23, the trends are similar, but the interaction strength is stronger. The most favourable adsorption site is equidistant to the imidazole ring and the ester group (3.3–3.4 Å). A similar geometry shows that the effect is not due to a different adsorption site or structure but the overall dispersion interaction with the framework. Up to $n = 3$, the average interaction decreases from 10 kcal mol^{-1} to 7 kcal mol^{-1} and then only negligibly fluctuates up to 23 CO_2 molecules which is in agreement with the observed experimental data (SI Chapter S3.2, Fig. S14). Subsequently, the change is less abrupt as the interaction slowly gets less favourable up to 32 CO_2 molecules, when it abruptly becomes repulsive (Fig. 8). Hence, NICS-23 can easily uptake 6.1 mmol/g CO_2 and not more than 8.4 mmol/g.

Experimental data for sorption were described with a Langmuir isotherm

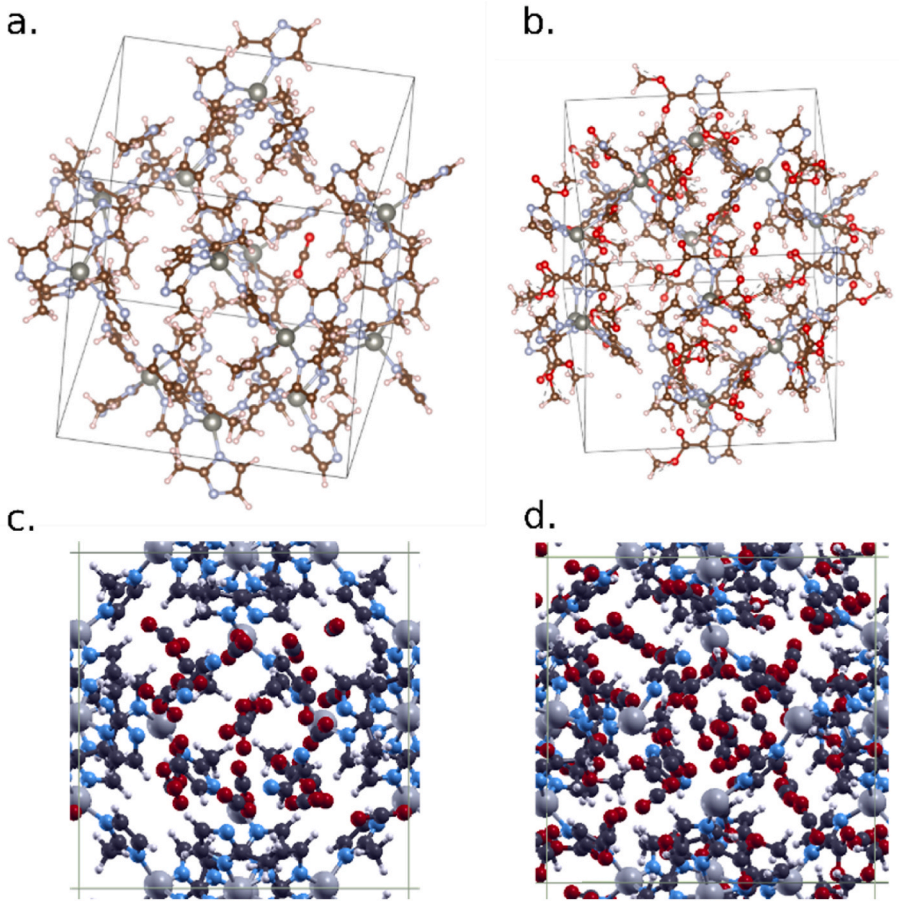

Fig. 8. Adsorption site for CO_2 in a) ZIF-8 and b) NICS-23. Full loading limit for c) ZIF-8 and d) NICS-23.

$$\theta = \frac{K_a P}{1 + K_a P}$$

where θ corresponds to the coverage, defined as a fraction of the maximum uptake (n/n_0, n_0 = 8.4 mmol/g), K_a is the corresponding equilibrium constant and P is pressure. For ZIF-8 and NICS-23, K_a is 0.0602 bar^{-1} and 0.1327 bar^{-1}, respectively, at 30 °C. This is consistent with different Gibbs free energies of adsorption for the two materials ($\Delta\Delta G = 4.61$ kcal mol^{-1}).

4. Conclusions

Mechanochemistry was successfully used to prepare a series of nine ZIFs with sodalite topology, with eight exhibiting permanent porosity. Of the prepared ZIFs, four were new phases of either known linker combinations or completely unknown phases. Among them NICS-23, the first reported ZIF with an ester group, was successfully prepared and its structure determined from PXRD. The eight porous ZIF structures were synthesized with high phase purity and moderate to high crystallinity. While a slight reduction of particle size of the obtained materials, compared to their solvothermal analogues was observed, the obtained particles exhibited similar agglomeration as in solvothermal synthesis.

CO_2, water and wet CO_2 isotherms of the eight materials were collected and evaluated, showing comparable sorption properties with their solvothermal counterparts, where available. The prepared materials could easily be divided into two groups the hydrophilic (ZIF-90, ZIF-94 and NICS-23) and hydrophobic (water uptake <1w%) (the rest). Dry CO_2 uptake confirmed the expected trends of more polar functional groups→ stronger interactions→ higher uptake, where the uptake was not limited by low porosity. Hydrophobic frameworks also exhibited retention of adsorption capacity in model wet CO_2, while all three hydrophilic structures showed competitive adsorption of water and CO_2.

Mechanochemistry proved again as a promising synthetic strategy for the preparation of various ZIF and ZIF-like materials with different functional groups, leading to fast and easy synthesis of novel materials, i.e. successfully addressing environmental and health issues of ZIFs solvothermal synthesis. The results demonstrated that the so-prepared materials can exhibit excellent dry and wet CO_2 performance, the impact of the latter often not properly or enough addressed in CO_2 sorption studies.

CRediT authorship contribution statement

Aljaž Škrjanc: Writing – original draft, Formal analysis, Data curation, Conceptualization. **Amalija Golobič:** Formal analysis. **Matjaž Mazaj:** Formal analysis. **Matej Huš:** Formal analysis. **Blaž Likozar:** Funding acquisition. **Nataša Zabukovec Logar:** Writing – review & editing, Supervision, Funding acquisition.

Data availability

The raw/processed data required to reproduce these findings cannot be shared at this time due to technical or time limitations. Raw adsorption data available upon request.

Declaration of competing interest

The authors declare that they have no known competing financial interests or personal relationships that could have appeared to influence the work reported in this paper.

Acknowledgements

The authors would like to thank Mojca Opresnik for SEM/EDX measurements, Tomaž Kotnik for ^{1}H NMR measurements, Jan Dežan for synthesis execution and Edi Kranjc for XRD measurements. This research was funded by the Slovenian Research and Innovation Agency Research programmes P1-0021, P2-0421 and P1-0175. M.H. further appreciates project funding J7-4638 and infrastructure funding I0-0039. Computational support was provided through the HPC RIVR consortium (www.hpc-rivr.si) and EuroHPC JU (eurohpc-ju.europa.eu) by providing the resources of the HPC system Vega at the Institute of Information Science, Maribor, Slovenia.

Appendix A. Supplementary data

Supplementary data to this article can be found online at https://doi.org/10.1016/j.micromeso.2024.113453.

Data availability

Data will be made available on request.

References

[1] M. Shahsavari, P.M. Jahani, I. Sheikhshoaie, S. Tajik, A.A. Afshar, M.B. Askari, P. Salarizadeh, A. Di Bartolomeo, H. Beitollahi, Green synthesis of zeolitic imidazolate frameworks: a review of their characterization and industrial and medical applications, Mater 15 (2022) 447, https://doi.org/10.3390/MA15020447, 15 (2022) 447.

[2] S. Kumar, S. Jain, M. Nehra, N. Dilbaghi, G. Marrazza, K.H. Kim, Green synthesis of metal–organic frameworks: a state-of-the-art review of potential environmental and medical applications, Coord. Chem. Rev. 420 (2020) 213407, https://doi.org/10.1016/j.ccr.2020.213407.

[3] H. Reinsch, M.A. Van Der Veen, B. Gil, B. Marszalek, T. Verbiest, D. De Vos, N. Stock, Structures, sorption characteristics, and nonlinear optical properties of a new series of highly stable aluminum MOFs, Chem. Mater. 25 (2013) 17–26, https://doi.org/10.1021/CM3025445/SUPPL_FILE/CM3025445_SI_004.CIF.

[4] M. Ghahramaninezhad, F. Mohajer, M. Niknam Shahrak, Improved CO2 capture performances of ZIF-90 through sequential reduction and lithiation reactions to form a hard/hard structure, Front. Chem. Sci. Eng. 14 (2020) 425–435, https://doi.org/10.1007/s11705-019-1873-5.

[5] W. Morris, B. Leung, H. Furukawa, O.K. Yaghi, N. He, H. Hayashi, Y. Houndonougbo, M. Asta, B.B. Laird, O.M. Yaghi, A combined Experimental−Computational investigation of carbon dioxide capture in a series of isoreticular zeolitic imidazolate frameworks, J. Am. Chem. Soc. 132 (2010) 11006–11008, https://doi.org/10.1021/ja104035j.

[6] Y. Ban, Y. Li, X. Liu, Y. Peng, W. Yang, Solvothermal synthesis of mixed-ligand metal–organic framework ZIF-78 with controllable size and morphology, Microporous Mesoporous Mater. 173 (2013) 29–36, https://doi.org/10.1016/J.MICROMESO.2013.01.031.

[7] T. Xu, W. Jiang, Y. Tao, M. Abdellatief, K.E. Cordova, Y.-B. Zhang, Popping and locking: balanced rigidity and porosity of zeolitic imidazolate frameworks for high-productivity methane purification, J. Am. Chem. Soc. 7 (2024) 22, https://doi.org/10.1021/JACS.4C00045.

[8] A.M. Bumstead, C. Castillo-Blas, I. Pakamorė, M.F. Thorne, A.F. Sapnik, A. M. Chester, G. Robertson, D.J.M. Irving, P.A. Chater, D.A. Keen, R.S. Forgan, T. D. Bennett, Formation of a meltable purinate metal–organic framework and its glass analogue, Chem. Commun. 59 (2023) 732–735, https://doi.org/10.1039/D2CC05314D.

[9] J. Yang, Y.W. Yang, Metal–organic frameworks for biomedical applications, Small 16 (2020) 1906846, https://doi.org/10.1002/SMLL.201906846.

[10] Y.R. Lee, M.S. Jang, H.Y. Cho, H.J. Kwon, S. Kim, W.S. Ahn, ZIF-8: a comparison of synthesis methods, Chem. Eng. J. 271 (2015) 276–280, https://doi.org/10.1016/J.CEJ.2015.02.094.

[11] M. García-Palacín, J.I. Martínez, L. Paseta, A. Deacon, T. Johnson, M. Malankowska, C. Téllez, J. Coronas, Sized-controlled ZIF-8 nanoparticle synthesis from recycled mother liquors: environmental impact assessment, ACS Sustain. Chem. Eng. 8 (2020) 2973–2980, https://doi.org/10.1021/acssuschemeng.9b07593.

[12] A. Škrjanc, C. Byrne, N. Zabukovec Logar, Green solvents as an alternative to DMF in ZIF-90 synthesis, Molecules 26 (2021) 1573, https://doi.org/10.3390/molecules26061573.

[13] J. Zhang, G.B. White, M.D. Ryan, A.J. Hunt, M.J. Katz, Dihydrolevoglucosenone (cyrene) as a green alternative to N,N -dimethylformamide (DMF) in MOF synthesis, ACS Sustain. Chem. Eng. 4 (2016) 7186–7192, https://doi.org/10.1021/acssuschemeng.6b02115.

[14] M. Bhindi, L. Massengo, J. Hammerton, M.J. Derry, S.D. Worrall, Structure control using bioderived solvents in electrochemical metal-organic framework synthesis, Appl. Sci. 13 (2023) 720, https://doi.org/10.3390/APP13020720, 13 (2023) 720.

[15] R.P. Lively, M.E. Dose, J.A. Thompson, B.A. McCool, R.R. Chance, W.J. Koros, Ethanol and water adsorption in methanol -derived ZIF-71, Chem. Commun. 47 (2011) 8667–8669, https://doi.org/10.1039/C1CC12728D.

[16] F.K. Shieh, S.C. Wang, S.Y. Leo, K.C.W. Wu, Water-based synthesis of zeolitic imidazolate framework-90 (ZIF-90) with a controllable particle size, Chem. Eur J. 19 (2013) 11139–11142, https://doi.org/10.1002/chem.201301560.

[17] E.V. Ramos-Fernandez, A. Grau-Atienza, D. Farrusseng, S. Aguado, A water-based room temperature synthesis of ZIF-93 for CO2 adsorption, J. Mater. Chem. A. 6 (2018) 5598–5602, https://doi.org/10.1039/C7TA09807C.
[18] V. Berned-Samatá, L. Martí Nez-Izquierdo, E. Abá, C. Té Llez Ab, J.N. Coronas, A facile route for the recovery of the ligand of zeolitic imidazolate framework ZIF-94/SIM-1, Chem. Commun. (2022), https://doi.org/10.1039/D2CC03661D.
[19] V. Martinez, T. Stolar, B. Karadeniz, I. Brekalo, K. Užarević, Advancing mechanochemical synthesis by combining milling with different energy sources, Nat. Rev. Chem 71 (7) (2022) 51–65, https://doi.org/10.1038/s41570-022-00442-1, 2022.
[20] I. Brekalo, W. Yuan, C. Mottillo, Y. Lu, Y. Zhang, J. Casaban, K.T. Holman, S. L. James, F. Duarte, P.A. Williams, K.D.M. Harris, T. Friščić, Manometric real-time studies of the mechanochemical synthesis of zeolitic imidazolate frameworks, Chem. Sci. 11 (2020) 2141–2147, https://doi.org/10.1039/C9SC05514B.
[21] F. Afshariazar, A. Morsali, The unique opportunities of mechanosynthesis in green and scalable fabrication of metal-organic frameworks, J. Mater. Chem. A. (2022), https://doi.org/10.1039/D2TA02699F.
[22] H.M. Titi, J.-L. Do, A.J. Howarth, K. Nagapudi, T. Friščić, Simple, scalable mechanosynthesis of metal–organic frameworks using liquid-assisted resonant acoustic mixing (LA-RAM), Chem. Sci. 11 (2020) 7578–7584, https://doi.org/10.1039/D0SC00333F.
[23] A.D. Katsenis, A. Puškarić, V. Štrukil, C. Mottillo, P.A. Julien, K. Užarević, M. H. Pham, T.O. Do, S.A.J. Kimber, P. Lazić, O. Magdysyuk, R.E. Dinnebier, I. Halasz, T. Friščić, In situ X-ray diffraction monitoring of a mechanochemical reaction reveals a unique topology metal-organic framework, Nat. Commun. 61 (6) (2015) 1–8, https://doi.org/10.1038/ncomms7662, 2015.
[24] J.L. Do, T. Friščić, Mechanochemistry: a force of synthesis, ACS Cent. Sci. 3 (2016) 13–19, https://doi.org/10.1021/ACSCENTSCI.6B00277.
[25] T. Stolar, K. Užarević, Mechanochemistry: an efficient and versatile toolbox for synthesis, transformation, and functionalization of porous metal–organic frameworks, CrystEngComm 22 (2020) 4511–4525, https://doi.org/10.1039/D0CE00091D.
[26] A. Sabetghadam, X. Liu, M. Benzaqui, E. Gkaniatsou, A. Orsi, M.M. Lozinska, C. Sicard, T. Johnson, N. Steunou, P.A. Wright, C. Serre, J. Gascon, F. Kapteijn, Influence of filler pore structure and polymer on the performance of MOF-based mixed-matrix membranes for CO2 capture, Chem. Eur J. 24 (2018) 7949–7956, https://doi.org/10.1002/CHEM.201800253.
[27] K. Zhong, R.F. Yang, W.Y. Zhang, Y.T. Yan, X.J. Gou, W.H. Huang, Y.Y. Wang, Zeolitic metal cluster carboxylic framework for selective carbon dioxide chemical fixation through the superlarge cage, ACS Appl. Mater. Interfaces (2020), https://doi.org/10.1021/acs.inorgchem.9b03581.
[28] M.E. Schweinefuß, S. Springer, I.A. Baburin, T. Hikov, K. Huber, S. Leoni, M. Wiebcke, Zeolitic imidazolate framework-71 nanocrystals and a novel SOD-type polymorph: solution mediated phase transformations, phase selection via coordination modulation and a density functional theory derived energy landscape, Dalt. Trans. 43 (2014) 3528–3536, https://doi.org/10.1039/C3DT52992D.
[29] M. Gao, J. Wang, Z. Rong, Q. Shi, J. Dong, A combined experimental-computational investigation on water adsorption in various ZIFs with the SOD and RHO topologies, RSC Adv. 8 (2018) 39627–39634, https://doi.org/10.1039/c8ra08460b.
[30] W. Gao, S. Wang, W. Zheng, W. Sun, L. Zhao, Computational evaluation of RHO-ZIFs for CO2 capture: from adsorption mechanism to swing adsorption separation, Sep. Purif. Technol. 313 (2023) 123469, https://doi.org/10.1016/J.SEPPUR.2023.123469.
[31] P. Kukkar, K.H. Kim, D. Kukkar, P. Singh, Recent advances in the synthesis techniques for zeolitic imidazolate frameworks and their sensing applications, Coord. Chem. Rev. 446 (2021) 214109, https://doi.org/10.1016/J.CCR.2021.214109.
[32] S. Tanaka, Y. Tanaka, A simple step toward enhancing hydrothermal stability of ZIF-8, ACS Omega 4 (2019) 19905–19912, https://doi.org/10.1021/ACSOMEGA.9B02812.
[33] F.A. Philip, A. Henni, Enhancement of post-combustion CO2 capture capacity by incorporation of task-specific ionic liquid into ZIF-8, Microporous Mesoporous Mater. (2021) 111580, https://doi.org/10.1016/J.MICROMESO.2021.111580.
[34] C.W. Chang, Y.H. Kao, P.H. Shen, P.C. Kang, C.Y. Wang, Nanoconfinement of metal oxide MgO and ZnO in zeolitic imidazolate framework ZIF-8 for CO2 adsorption and regeneration, J. Hazard Mater. 400 (2020) 122974, https://doi.org/10.1016/j.jhazmat.2020.122974.
[35] H.N. Abdelhamid, Dye encapsulated hierarchical porous zeolitic imidazolate frameworks for carbon dioxide adsorption, J. Environ. Chem. Eng. 8 (2020) 104008, https://doi.org/10.1016/j.jece.2020.104008.
[36] A. Škrjanc, M. Opresnik, M. Gabrijelčič, A. Šuligoj, G. Mali, N. Zabukovec Logar, Impact of dye encapsulation in ZIF-8 on CO2, water, and wet CO2 sorption, Mol 28 (2023) 7056, https://doi.org/10.3390/MOLECULES28207056, 28 (2023) 7056.
[37] M. Åhlén, A. Jaworski, M. Strømme, O. Cheung, Selective adsorption of CO2 and SF6 on mixed-linker ZIF-7–8s: the effect of linker substitution on uptake capacity and kinetics, Chem. Eng. J. 422 (2021) 130117, https://doi.org/10.1016/J.CEJ.2021.130117.
[38] Y.W. Abraha, F.J.F. Jacobs, A. Brink, E.H.G. Langner, Effect of solvent assisted linker exchange (SALE) and de novo synthetic routes on CO2 uptake and fixation by mixed-linker zeolitic imidazolate frameworks, J. Inorg. Organomet. Polym. Mater. 1 (2023) 1–17, https://doi.org/10.1007/S10904-023-02653-5/TABLES/5.
[39] Z. Jiang, W. Xue, H. Huang, H. Zhu, Y. Sun, C. Zhong, Mechanochemistry-assisted linker exchange of metal-organic framework for efficient kinetic separation of propene and propane, Chem. Eng. J. 454 (2023) 140093, https://doi.org/10.1016/j.cej.2022.140093.
[40] W. Morris, N. He, K.G. Ray, P. Klonowski, H. Furukawa, I.N. Daniels, Y. A. Houndonougbo, M. Asta, O.M. Yaghi, B.B. Laird, A combined experimental-computational study on the effect of topology on carbon dioxide adsorption in zeolitic imidazolate frameworks, J. Phys. Chem. C 116 (2012) 24084–24090, https://doi.org/10.1021/jp307170a.
[41] S.K. Nune, P.K. Thallapally, A. Dohnalkova, C. Wang, J. Liu, G.J. Exarhos, Synthesis and properties of nano zeolitic imidazolate frameworks, Chem. Commun. 46 (2010) 4878–4880, https://doi.org/10.1039/C002088E.
[42] Y. Choi, K. Noh, J. Lee, J. Kim, Porosity properties of the conformers of sodalite-like zeolitic imidazolate frameworks, J. Am. Chem. Soc. 140 (2018) 14586–14589, https://doi.org/10.1021/jacs.8b08997.
[43] J. Liu, X. Tang, X. Liang, L. Wu, F. Zhang, Q. Shi, J. Yang, J. Dong, J. Li, Superhydrophobic zeolitic imidazolate framework with suitable SOD cage for effective CH4/N2 adsorptive separation in humid environments, AIChE J. (2022) e17589, https://doi.org/10.1002/AIC.17589.
[44] L.H. Wee, S. Vandenbrande, S.M.J. Rogge, J. Wieme, K. Asselman, E.O. Jardim, J. Silvestre-Albero, J.A.R. Navarro, V. Van Speybroeck, J.A. Martens, C.E. A. Kirschhock, Chlorination of a Zeolitic-Imidazolate Framework Tunes Packing and van der Waals Interaction of Carbon Dioxide for Optimized Adsorptive Separation, J. Am. Chem. Soc. 143 (2021) 4962–4968, https://doi.org/10.1021/JACS.0C08942.
[45] K. Li, D.H. Olson, J. Seidel, T.J. Emge, H. Gong, H. Zeng, J. Li, Zeolitic imidazolate frameworks for kinetic separation of propane and propene, J. Am. Chem. Soc. 131 (2009) 10368–10369, https://doi.org/10.1021/ja9039983.
[46] S. Diring, D.O. Wang, C. Kim, M. Kondo, Y. Chen, S. Kitagawa, K.I. Kamei, S. Furukawa, Localized cell stimulation by nitric oxide using a photoactive porous coordination polymer platform, Nat. Commun. 41 (4) (2013) 1–8, https://doi.org/10.1038/ncomms3684, 2013.
[47] M. Švegovec, A. Škrjanc, A. Krajnc, N.Z. Logar, Green synthesis approaches toward preparation of ZIF-76 and its thermal behavior, Cryst. Growth Des. 23 (2023) 3754–3760, https://doi.org/10.1021/acs.cgd.3c00137.
[48] G. Kresse, J. Hafner, *Ab initio* molecular dynamics for liquid metals, Phys. Rev. B 47 (1993) 558, https://doi.org/10.1103/PhysRevB.47.558.
[49] G. Kresse, J. Furthmüller, Efficient iterative schemes for *ab initio* total-energy calculations using a plane-wave basis set, Phys. Rev. B 54 (1996) 11169, https://doi.org/10.1103/PhysRevB.54.11169.
[50] G. Kresse, J. Hafner, *Ab initio* molecular-dynamics simulation of the liquid-metal–amorphous-semiconductor transition in germanium, Phys. Rev. B 49 (1994) 14251, https://doi.org/10.1103/PhysRevB.49.14251.
[51] B. Hammer, L.B. Hansen, J.K. Nørskov, Improved adsorption energetics within density-functional theory using revised Perdew-Burke-Ernzerhof functionals, Phys. Rev. B 59 (1999) 7413, https://doi.org/10.1103/PhysRevB.59.7413.
[52] G. Kresse, D. Joubert, From ultrasoft pseudopotentials to the projector augmented-wave method, Phys. Rev. B 59 (1999) 1758, https://doi.org/10.1103/PhysRevB.59.1758.
[53] S. Grimme, J. Antony, S. Ehrlich, H. Krieg, A consistent and accurate ab initio parametrization of density functional dispersion correction (DFT-D) for the 94 elements H-Pu, J. Chem. Phys. 132 (2010), https://doi.org/10.1063/1.3382344/926936.
[54] A. Kundu, K. Sillar, J. Sauer, Ab initio prediction of adsorption isotherms for gas mixtures by grand canonical Monte Carlo simulations on a lattice of sites, J. Phys. Chem. Lett. 8 (2017) 2713–2718, https://doi.org/10.1021/acs.jpclett.7b01205.
[55] N. Missaoui, M. Bouzid, A. Chrouda, H. Kahri, H. Barhoumi, A.L. Pang, M. Ahmadipour, Interpreting of the carbon dioxide adsorption on high surface area zeolitic imidazolate Framework-8 (ZIF-8) nanoparticles using a statistical physics model, Microporous Mesoporous Mater. 360 (2023) 112711, https://doi.org/10.1016/J.MICROMESO.2023.112711.
[56] X. Wu, J. Huang, W. Cai, M. Jaroniec, Force field for ZIF-8 flexible frameworks: atomistic simulation of adsorption, diffusion of pure gases as CH 4 , H 2 , CO 2 and N 2, RSC Adv. 4 (2014) 16503–16511, https://doi.org/10.1039/C4RA00664J.
[57] H. Amrouche, S. Aguado, J. Pérez-Pellitero, C. Chizallet, F. Siperstein, D. Farrusseng, N. Bats, C. Nieto-Draghi, Experimental and computational study of functionality impact on sodalite-zeolitic imidazolate frameworks for CO2 separation, J. Phys. Chem. C 115 (2011) 16425–16432, https://doi.org/10.1021/jp202804g.
[58] D.A. (Donald A. McQuarrie, Physical Chemistry : a Molecular Approach, University Science Books, Sausalito, Calif, 1997. ©1997, n.d. https://search.library.wisc.edu/catalog/999849410402121.
[59] S. Springer, I.A. Baburin, T. Heinemeyer, J.G. Schiffmann, L. Van Wüllen, S. Leoni, M. Wiebcke, A zeolitic imidazolate framework with conformational variety: conformational polymorphs versus frameworks with static conformational disorder, CrystEngComm 18 (2016) 2477–2489, https://doi.org/10.1039/C6CE00312E.
[60] S. Zhou, Y. Wei, L. Li, Y. Duan, Q. Hou, L. Zhang, L.-X. Ding, J. Xue, H. Wang, J. Caro, Paralyzed membrane: current-driven synthesis of a metal-organic framework with sharpened propene/propane separation. https://www.science.org, 2018. (Accessed 12 April 2024).
[61] N. Masciocchi, F. Castelli, P.M. Forster, M.M. Tafoya, A.K. Cheetham, Synthesis and characterization of two polymorphic crystalline phases and an amorphous powder of nickel(II) bisimidazolate, Inorg. Chem. 42 (2003) 6147–6152, https://doi.org/10.1021/ic034619o.
[62] Q.-F. Yang, X.-B. Cui, J.-H. Yu, J. Lu, X.-Y. Yu, X. Zhang, J.-Q. Xu, Q. Hou, T.-G. Wang, A series of metal–organic complexes constructed from in situ generated

organic amines, CrystEngComm 10 (2008) 1534–1541, https://doi.org/10.1039/B806980H.
[63] R. Bose, V. Bon, N. Bönisch, P. Selvam, N.S. Kaisare, S. Kaskel, Crystal size dependent flexibility in ZIF-7: from macro- to nanoscale, Chem. Mater. (2023), https://doi.org/10.1021/ACS.CHEMMATER.3C01840.
[64] Q. Jia, E. Lasseuguette, M.M. Lozinska, M.-C. Ferrari, P.A. Wright, Hybrid benzimidazole–dichloroimidazole zeolitic imidazolate frameworks based on ZIF-7 and their application in mixed matrix membranes for CO2/N2 separation, ACS Appl. Mater. Interfaces (2022), https://doi.org/10.1021/ACSAMI.2C12908.
[65] C. Byrne, A. Ristić, S. Mal, M. Opresnik, N.Z. Logar, Evaluation of ZIF-8 and ZIF-90 as heat storage materials by using water, methanol and ethanol as working fluids, Cryst 11 (2021) 1422, https://doi.org/10.3390/CRYST11111422, 11 (2021) 1422.
[66] Q. Wang, Y. Chen, P. Liu, Y. Wang, J. Yang, J. Li, L. Li, CO2 capture from high-humidity flue gas using a stable metal–organic framework, Mol. 27 (2022) 5608, https://doi.org/10.3390/MOLECULES27175608, 27 (2022) 5608.
[67] M. Fischer, R.G. Bell, Interaction of hydrogen and carbon dioxide with sod -type zeolitic imidazolate frameworks: a periodic DFT-D study, CrystEngComm 16 (2014) 1934–1949, https://doi.org/10.1039/C3CE42209G.
[68] H.P. Paudel, W. Shi, D. Hopkinson, J.A. Steckel, Y. Duan, Computational modelling of adsorption and diffusion properties of CO 2 and CH 4 in ZIF-8 for gas separation applications: a density functional theory approach, React. Chem. Eng. 6 (2021) 990–1001, https://doi.org/10.1039/d0re00416b.